Arch. Min. Sci. **71** (2026), 2, 199-218

Electronic version (in color) of this paper is available: http://mining.archives.pl

DOI: https://doi.org/10.24425/ams.2026.158813

JUHYI YIM[1], JAE HOON JUNG[1], HAN BYUL KANG[1],
YOUNG JIN SHIN[1*]

DESIGN AND FIELD-SCALE DEMONSTRATION OF PRE-FRACTURING WITH A PRACTICAL MODEL FOR THE SIZE ESTIMATION OF BLAST-INDUCED DAMAGED ZONE

Pre-fracturing is introduced as an auxiliary method for mechanical excavation, aiming to weaken the hard rock and control the Excavated Damaged Zone (EDZ). Pre-fracturing necessitates re-optimised charge and hole layouts due to its objectives, which differ from conventional single-free-face blasting. This motivates a rigorous estimator of the blast-damage extent surrounding a blast hole. A practical model for estimating the Blast-Induced Damaged Zone (BIDZ) around a blast hole was analytically derived under quasi-static conditions while accounting for dynamic rock strength, in-situ stress, spherical symmetry, and blast-induced changes in hole radius. The validity of the practical model was confirmed via comparisons with dynamic numerical models, empirical relations, and experimental data from previous research. The practical model shows good agreement with empirical relations and reproduces trends observed in dynamic numerical simulations, with discrepancies below 45% across the tested conditions. Based on experimental data, the maximum crack length from a blast hole was approximately 1.3 times the BIDZ estimated by the practical model. A field-scale demonstration of pre-fracturing was conducted on a hard-rock quarry slope. Rock weakening with decreasing hole spacing was verified through surface observations and laboratory tests. The EDZ extent was effectively controlled to 9-10 cm from the contour, which is below the typical extent produced by the conventional excavation method. Based on the pre-splitting cases and the present field-demonstration, the optimal hole spacing was proposed as 1.5-3.0 times the BIDZ estimated by the practical model. A blast-pattern design for pre-fracturing is also suggested, considering the optimal hole spacing and maximum crack length estimate based on the practical model.

Keywords: Excavated Damaged Zone (EDZ); Blast-Induced Damaged Zone (BIDZ); Pre-fracturing; Preconditioning; Damage zone; Field-scale demonstration

[1] R&D DIVISION, HYUNDAI ENGINEERING AND CONSTRUCTION, 75, YULGOK-RO, JONGNO-GU, SEOUL, REPUBLIC OF KOREA

* Corresponding author: johnyj.shin@hdec.co.kr

1. Introduction

As urban densification intensifies, the demand for underground space continues to increase, and such infrastructure has traditionally been constructed using blasting methods. To address public complaints and safety concerns in urban areas, mechanical excavation has been increasingly adopted. Applications such as deep geological disposal repositoriesoften require mechanical excavation because it offers low vibration, reduced noise, and a small excavation damaged zone (EDZ). However, excavating hard rock with a strength exceeding 100 MPa reduces penetration rates and accelerates cutter wear, thereby lowering productivity. Consequently, a pre-fracturing method has been developed to induce fractures in the hard-rock face using small explosive charges before mechanical excavation, thereby increasing productivity and controlling the extent of EDZ.

Pre-fracturing is distinct from other conventional single-free-face blasting methods for hard rock, such as pre-blasting, destress blasting, and pre-splitting, as shown in TABLE 1. Pre-blasting is used to facilitate ripping and excavation [1,2], to penetrate boulders during shield tunnelling [3], or to weaken the unconsolidated confined aquifer above the coal seam [4]. Destress blasting, typically applied in highly stressed deep underground, relieves the stress concentration to prevent rockbursts [5-7]. Pre-splitting is designed to create fracture planes between closely spaced blast holes. These conventional methods have predominantly relied on empirical design approaches. To date, no research on the detailed design of pre-blasting has been reported, likely because the sole purpose is rock weakening. The effectiveness of destress blasting has only recently been analysed numerically [8]. Pre-splitting often adopts simple empirical rules, such as setting the hole spacing at 12 times the blast-hole diameter [9] or employing formulas that account for tensile strength and borehole wall pressure [10]. However, pre-fracturing requires precise design considerations to balance the dual objectives: weakening the rock face and controlling EDZ. The hole spacing of pre-fracturing can exceed that used for pre-splitting, as the creation of a fracture plane is not required. Conversely, the hole configuration is denser than that used for destress blasting, as the entire tunnel face needs to be sufficiently weakened. This necessitates rigorous analyses beyond empirical estimations to optimise the explosive charge and hole configurations, considering properties of both explosives and surrounding rocks.

A pre-fracturing design framework can be developed by determining the crack length from a blast hole, referred to here as the Blast-Induced Damaged Zone (BIDZ). This parameter can be directly correlated to the hole spacing. The BIDZ can be estimated using peak particle velocity (PPV), a widely used approach [11]; however, the parameters required for this approach can only be determined after test blasting. Alternatively, property-based formulas avoid testing, yet many are limited by oversimplified fracture models or omission of rock strength [12-15]. Ouchterlony [16] developed an equation for BIDZ that avoids the need for test blasting, uncommon laboratory tests, or extreme simplification, but it relies on empirical parameters fitted to limited data. Numerical methods have been utilised to simulate the fracture mechanism and estimate the BIDZ. Although advances in computing have made numerical simulations more feasible, it is often impractical to rely on high-fidelity analyses alone to explore the full design space, because substantial effort is still required for parameter specification, model set-up, and verification/validation. Therefore, for effective design of pre-fracturing by filling the gap of knowledge, a practical and validated method for estimating BIDZ is needed.

This study introduces pre-fracturing as an auxiliary method for mechanical excavation and evaluates its application on a hard-rock quarry slope. The first objective is to develop and validate a practical, quasi-static model for estimating the BIDZ from a single blast hole, accounting for dynamic rock strength, blasting-induced hole-radius change, spherical symmetry of a concentrated charge, and in-situ stress; the plausibility of the quasi-static assumption is also addressed. The second objective is to translate this model into a design methodology for pre-fracturing to weaken the rock face and control the EDZ. The working hypotheses are that (i) the practical BIDZ model is adequate for design when benchmarked against established dynamic numerical models and empirical relations, (ii) the practical BIDZ model can be used to estimate the maximum crack length, which can be regarded as EDZ, and (iii) a BIDZ-based hole-spacing threshold exists such that rock-face weakening occurs only when spacing is below that threshold. The research questions are how the BIDZ estimate relates to EDZ and what BIDZ-normalised threshold governs the occurrence of weakening. Model validity is examined through comparisons with dynamic simulations and empirical relations, and the link between BIDZ and maximum crack length is established using experimental data from previous studies. A field-scale demonstration is then used to determine the BIDZ-normalised hole-spacing threshold for weakening: spacing-dependent rock-face weakening is documented by surface observations and laboratory tests, and EDZ control is assessed using PPV data. Because the EDZ generated by mechanical excavation is limited relative to blasting, pre-fracturing was not followed by mechanical excavation, and the damaged zone produced by pre-fracturing is regarded as EDZ in this study. Finally, the study proposes hole-spacing ranges and blast patterns for effective pre-fracturing.

TABLE 1

The comparison of pre-fracturing against general blasting and pre-splitting

	Pre-existing blasting			Pre-fracturing
	General blasting	Pre-splitting	Destress Blast	
Purpose	Excavation	Fracture plane generation	Relieve stress concentration	Rock weakening & EDZ control
Excavation	Drill and Blast	Drill and Blast	Drill and Blast	Mechanical excavation
Noise&Vibration Tolerance	High	High	High	Low
Number of free face	2	1	1	1
Hole spacing	Wide	Narrow	Very wide	Less narrow
Hole distribution	Whole face	Contour	Partly around corner and face	Whole face
Blast design	Empirical models by Hauser, Langefors, and etc.	Empirical model	Empirical model	Not established

2. Size estimation of blast-induced damaged zone

2.1. Practical model

The crack length induced by blasting, defined as BIDZ in this study, can be analytically evaluated considering the properties of the explosive and the rock. According to Persson et al. [17], the pressure in the borehole wall decreases due to the high decoupling ratio, and the borehole pressure (P_0) is given by Eq. (1). The value of a typically ranges from 2.0 to 2.6 [16,18-21]. In this paper, a value of 2.2 is used.

$$P_0 = \frac{\gamma^{\gamma}}{(\gamma+1)^{\gamma+1}} \rho_e VOD^2 \left(\frac{r_e}{a_0}\right)^a \tag{1}$$

where γ is adiabatic expansion exponent; ρ_e is explosive density (kg/m^3); VOD is the velocity of detonation (m/s); r_e is the radius of explosive; a_0 is the radius of the borehole. Adiabatic expansion exponent can be estimated as Eq. (2) [22].

$$\gamma = \sqrt{1 + \frac{VOD^2}{2e}} \tag{2}$$

where VOD is the velocity of detonation (m/s), e is the reaction heat of the explosive.

In this paper, a quasi-static state is assumed, and analytic formulas are derived by dividing the region from near the hole into the compressive failure zone ($a_0 \sim r_{crushed}$), the tensile failure zone ($r_{crushed} \sim r_{crack}$), and the elastic zone ($r_{crack} \sim \infty$) [12,13,23,24]. This assumption is consistent with recent experimental work on saturated granite that maps early-stage clustering of tensile-mode micro-cracks and a subsequent transition to shear-dominated failure near global instability [25]. First, under the conditions of cylindrical symmetry and plane strain, the force equilibrium equation is given by Eq. (3).

$$\frac{d\sigma_r}{dr} + \frac{\sigma_r - \sigma_\theta}{r} = 0 \tag{3}$$

where σ_r is the radial stress; σ_θ is the tangential stress; r is the radial coordinate centered at the hole center.

Considering that displacement and strain are zero at infinity and $\sigma_r(r = r_{crack}) = \sigma_{t,dynamic} + 2S$, the radial displacement at r_{crack} can be obtained using the elastic solution, as shown in Eq. (4).

$$u(r_{crack}, t) = \frac{(\sigma_{t,dynamic} + 2S) r_{crack}(t)}{2\mu} \tag{4}$$

where r_{crack} is the distance from the hole center to the boundary of the tensile failure zone; $\sigma_{t,dynamic}$ is the dynamic tensile strength; S is isotropic in-situ stress; $\mu = \left(\frac{E}{2(1+\nu)}\right)$ is dynamic shear modulus; t represents a certain time after the explosion.

In the tensile failure zone, due to the development of radial cracks, the condition, $\sigma_\theta = 0$, can be applied. By using the condition of $\sigma_r(r = r_{crushed}) = \sigma_c$, Eqs. (5)-(6) are derived as below.

$$(\sigma_{t,dynamic} + 2S) r_{crack} = \sigma_c r_{crushed} \tag{5}$$

$$u(a,t)=\frac{\sigma_c r_{crushed}^2(t)}{2\mu a}\left[1+\ln\frac{\sigma_c}{\sigma_{t,dynamic}+2S}\right] \tag{6}$$

where $r_{crushed}$ is the distance from the hole center to the boundary of the compressive failure zone; σ_c is the compressive strength; a is the expanded hole radius; u is the radial displacement.

Under the assumption of $\frac{\partial u}{\partial a}\approx 0$, $da/dt = du/dt \approx \left(\frac{\partial u}{\partial r_{crushed}}\right)\left(\frac{\partial r_{crushed}}{\partial t}\right)$ and $a(t=0) = r_{crushed}(t=0) = a_0$. Solving this, Eqs. (7)-(8) can be derived as below. For compactness, L_{2D} is defined in Eq. (7)

$$L_{2D}=\frac{\mu}{\sigma_c\left(1+\ln\left(\frac{\sigma_c}{\sigma_{t,dynamic}+2S}\right)\right)} \tag{7}$$

$$r_{crushed}=a_0\left[L_{2D}\left(\frac{a_0}{a}\right)^{-2}+\left(1-L_{2D}\right)\right]^{\frac{1}{2}} \tag{8}$$

In the compressive failure zone, where the radial and tangential stress are the principal stresses, Coulomb's law ($\tau = -\sigma_n \tan\phi + c$) is satisfied, leading to failure. Combining this with the force equilibrium equation, Eq. (9) is obtained.

$$\sigma_r=\frac{c}{\tan\phi}-\left(\sigma_c+\frac{c}{\tan\phi}\right)\left(\frac{r_{crushed}}{a}\right)^{\frac{2\sin\phi}{1+\sin\phi}} \tag{9}$$

where c is cohesion; ϕ is friction angle.

Unlike previous studies that ignored the change of borehole radius ($a_0 = a$), this study assumes thermal expansion of explosive gas from a_0 to a, and derives Eq. (10).

$$P_0\left(\frac{a_0}{a}\right)^{2\gamma}=-\frac{c}{\tan\phi}+\left(\sigma_c+\frac{c}{\tan\phi}\right)\left(L_{2D}+\left(1-L_{2D}\right)\left(\frac{a_0}{a}\right)^2\right)^{\frac{\sin\phi}{1+\sin\phi}} \tag{10}$$

If the borehole pressure does not exceed the compressive strength, the compression failure zone does not form. However, if it exceeds the compressive strength, the ratio a_0/a satisfying Eq. (10) must be determined. It can be determined by the iterative method. Consequently, the BIDZ corresponding to r_{crack} is given by Eq. (11).

$$r_{crack}\,|_{2D}=\begin{cases}\dfrac{\sigma_c}{\sigma_{t,dynamic}+2S}r_{crushed} & \left(P_0\geq\sigma_c\right)\\[2ex] \dfrac{P_0}{\sigma_{t,dynamic}+2S}a_0 & \left(\sigma_{t,dynamic}+S<P_0<\sigma_c\right)\end{cases} \tag{11}$$

If the explosive charge is concentrated at a point, spherical symmetry may be valid. In this case, the force equilibrium equation is given by Eq. (12).

$$\frac{d\sigma_r}{dr}+\frac{2\left(\sigma_r-\sigma_\theta\right)}{r}=0 \tag{12}$$

Under the aforementioned assumptions, we obtain the following solutions with $\sigma_r(r=r_{crack}) = 2\sigma_{t,dynamic} + 3S$: Eqs. (13)-(16). For compactness, L_{3D} is defined in Eq. (13).

$$L_{3D}=\frac{2\mu}{3\sigma_c\left(1-\sqrt{\dfrac{2\sigma_{t,dynamic}+3S}{2\sigma_c}}\right)} \tag{13}$$

$$P_0\left(\frac{a_0}{a}\right)^{3\gamma}=-\frac{c}{\tan\phi}+\left(\sigma_c+\frac{c}{\tan\phi}\right)\left(L_{3D}+\left(1-L_{3D}\right)\left(\frac{a_0}{a}\right)^3\right)^{\frac{4\sin\phi}{3(1+\sin\phi)}} \tag{14}$$

$$r_{crushed}=a_0\left[L_{3D}\left(\frac{a_0}{a}\right)^{-3}+\left(1-L_{3D}\right)\right]^{\frac{1}{3}} \tag{15}$$

$$r_{crack}\,|_{3D}=\begin{cases}\left(\dfrac{\sigma_c}{2\sigma_{t,dynamic}+3S}\right)^{\frac{1}{2}} r_{crushed} & \left(P_0\geq\sigma_c\right)\\[2ex] \left(\dfrac{P_0}{2\sigma_{t,dynamic}+3S}\right)^{\frac{1}{2}} a_0 & \left(P_0<\sigma_c\right)\end{cases} \tag{16}$$

In hard rock, it has been observed that the initial pressure from the explosive is maintained for several milliseconds, and it takes approximately 0.5 ms to reach this initial pressure [26]. In this study, it is assumed that 0.3 ms is required to reach the initial pressure at the borehole wall. Thus, the strain rate ($\dot{\varepsilon}$) at the end of the crack can be estimated as Eq. (17).

$$\dot{\varepsilon}=\begin{cases}\dfrac{S+\sigma_{t,dynamic}}{0.0003\left(2\mu\right)} & \left(2-dimension\right)\\[2ex] \dfrac{S+\sigma_{t,dynamic}}{0.0003\left(\mu\right)} & \left(3-dimension\right)\end{cases} \tag{17}$$

In general application, the strain rate in Eq. (17) is in the range of 10^{-1}~10^{1}, where quasi-static state assumption can be applied. Although the compressive strength does not vary significantly within this range [27,28], the tensile strength shows a significant difference. Therefore, the Cowper-Symonds strain rate model, as shown in Eq. (18), was employed to determine the dynamic tensile strength, with D and p values set to 10 and 6, respectively [29].

$$\frac{\sigma_{t,static}}{\sigma_{t,dynamic}}=1+\left(\frac{\dot{\varepsilon}}{D}\right)^{\frac{1}{p}} \tag{18}$$

There are various rock-related properties that influence crack propagation, including saturation and mineral composition. For example, saturation increases internal energy dissipation during rock failure, thereby amplifying damage [30]. Because these factors modify key material properties such as strength and stiffness [31-33], their effects can be indirectly incorporated into the practical BIDZ model by parameterising those properties. Further experimental data and validation on these aspects are needed as future work.

2.2. Empirical model

The CANMET Pit Slope Manual [34] proposed the following design relationship of hole spacing, s, for pre-splitting, as stated in Eq. (19) [10].

$$\frac{s}{2a_0} \leq \frac{P_o + \sigma_{t,dynamic}}{\sigma_{t,dynamic}} = \frac{P_o}{\sigma_{t,dynamic}} + 1 \tag{19}$$

The Swedish National Road Administration (SNRA) suggested a table correlating the damage zone depth, corresponding to the BIDZ, to the charge concentration of Dynamex (q) [15], based on the experiments by Sjöberg [35,36]. The SNRA table is empirically accepted and widely used by many experts. It matches well with the widely used model by Holmberg and Persson [11,37,38]. Ouchterlony et al. [38] proposed Eq. (20) fitting the SNRA table.

$$r_{crack} = \begin{cases} 1.9q & \left(q < 0.5\dfrac{\text{kg}}{\text{m}}\right) \\ 0.95(q+0.5) & \left(0.5 \leq q \leq 1.6\dfrac{\text{kg}}{\text{m}}\right) \end{cases} \tag{20}$$

Swedish Rock Engineering Research Foundation (Stiftelsen Svensk Bergteknisk Forskning, SveBeFo) directly measured the maximum crack radius according to the charge density of the outermost hole in bench blasting performed at the Vånga quarry [10,39-41]. By fitting this data, Ouchterlony [16] proposed an empirical formula considering the characteristics of the explosive and the fracture mechanics properties of the rock (Eq. (21)).

$$r_{crack} = a_0 \left(\frac{P_0}{P_{crack}}\right)^{\frac{2}{3\left(\frac{VOD}{V_p}\right)^{0.25} - 1}} \qquad \left(P_{crack} = 3.30\frac{K_{IC}}{\sqrt{2a_0}}\right) \tag{21}$$

where V_P is p-wave velocity of rock, and K_{IC} is mode 1 fracture toughness of rock.

2.3. Validation of practical model

2.3.1. Comparison with numerical models

Numerical analyses from previous studies incorporating the dynamic effect and the Jones–Wilkins-Lee equation show reasonable agreement with the results of the practical model used in this study. Yang et al. [42] and Saadatmand Hashemi and Katsabanis [8] used LS-DYNA, and the 2D model with emulsion and the 3D model with ANFO were established, respectively. Comparison of the BIDZ estimated by the practical and numerical models, as shown in Fig. 1, indicates a similar trend with respect to in-situ stress, with discrepancies less than 45% observed in stress ranges below 50 MPa. In addition, because of the uncertainty of numerical models, the evaluation of which model more accurately represents reality should be conducted through comparisons with empirical measurements.

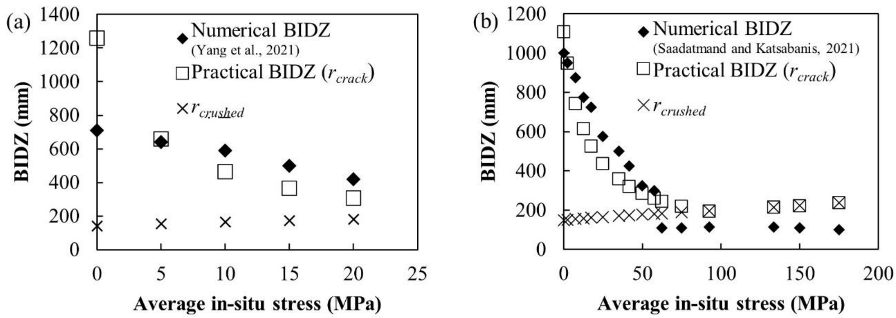

Fig. 1. The comparison between the practical and numerical BIDZ according to (a) Yang et al. [42] and (b) Saadatmand Hashemi and Katsabanis [8]

2.3.2. Comparison with empirical relations and experimental data

Firstly, the practical model is approximately identical to the CANMET design relationship. Under the condition of no in situ-stress, cylindrical symmetry and the borehole pressure below compressive strength, Eq. (19) can be transformed into Eq. (11) if $s = 2r_{crack}$ and $P_0/\sigma_{t,dynamic} \gg 1$. It means that the newly derived estimation is essentially consistent with the conventional formula.

The practical model is also validated by matching with the SNRA table, as shown in Fig. 2. It indicates that the estimation of borehole pressure and dynamic tensile strength is applicable. The general properties of Swedish granite in TABLE 2 were used. The branch point of two graphs at around 0.5 kg/m is due to the large borehole pressure over compressive strength. As the practical model underestimates the BIDZ after 0.5 kg/m, it is inferred that conditions ignored in the practical model, such as thermo-dynamic effect, become significant.

TABLE 2

Properties of Swedish granite and Dynamex [43] for SNRA table

Uniaxial compressive strength (MPa)	Tensile strength (MPa)	Dynamic Young's modulus (GPa)	Dynamic Poisson's ratio	Internal friction angle (°)	Cohesion (MPa)	Rock density (kg/m^3)	P-wave velocity (m/s)
200*	12*	76†	0.25†	49†	37.4‡	2750†	5759‡

Unexploded explosive density (kg/m^3)	Ideal detonation velocity (m/s)	Complete reaction heat (kJ/kg)	Hole radius (mm)	Charge radius (mm)
1400	5000	4500	25	3.1

(*Vånga granite [41], †Äspö granite [44], ‡calculated)

The maximum crack lengths were measured in field experiments conducted in Sweden and Finland [10,39-41,45,46]. Fig. 3 shows a comparison of measured maximum crack lengths with

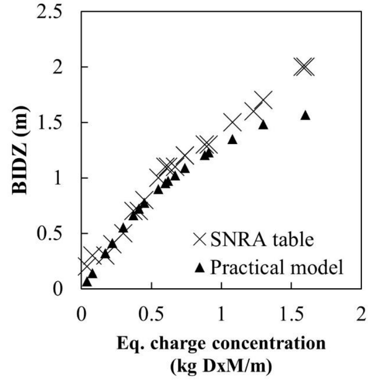

Fig. 2. Size estimation of blast-induced damaged zone by SNRA table and practical model

BIDZ estimated by the practical model (Eq. (11) or Eq. (16) and empirical models by SNRA table (Eq. (20)) and Ouchterlony [16] (Eq. (21)). When fracture toughness was not provided, it was estimated using an empirical relationship with rock properties [47]. For model comparison considering the heteroscedasticity, the coefficients of variation for the measured-to-estimated

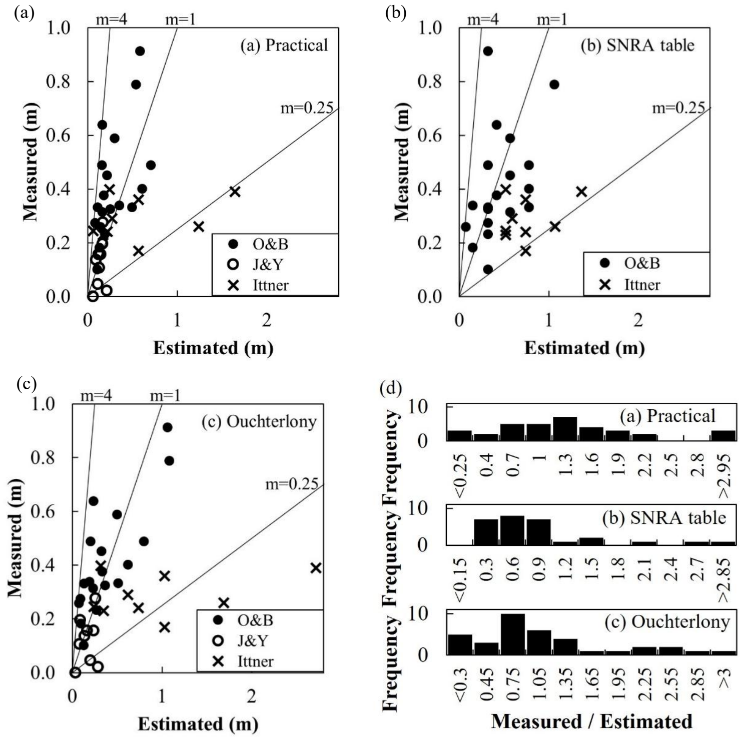

Fig. 3. Comparison of maximum crack length against estimated values by (a) practical model, (b) SNRA table, (c) Ouchterlony's model

values using the practical model, SNRA table, and Ouchterlony [16] were calculated as 0.66, 0.81, and 0.73 (TABLE 3), respectively, indicating comparable correlations between the practical and empirical models. The measured maximum crack length was approximately 1.3 times greater than the BIDZ estimated by the practical model, likely attributable to rock strength heterogeneity. One thing to note is that most of the data in Fig. 2 were measured in the low stress range close to 0, where the numerical model relatively underestimates the BIDZ with respect to the practical model.

TABLE 3

Coefficient of variation for the measured-to-estimated values

In-situ stress	Practical model	SNRA table	Ouchterlony's model
Total	0.66	0.81	0.73
over 0.9 MPa	0.94	0.38	0.75
near 0 MPa	0.57	0.69	0.62

2.4. Sensitivity analysis of practical model

A sensitivity analysis of the practical BIDZ model was performed (Figs. 4-5). Baseline rock-mass and explosive properties were taken from PF-2 of the field-scale experiment in this study (TABLE 4). As UCS increases, the crushed zone contracts, and as tensile strength increases, BIDZ decreases sharply. The internal friction angle and dynamic elastic modulus have only minor effects. A column charge produces a larger BIDZ than a concentrated charge, and the influence of hole radius acts in opposite directions for the two charge types. To clarify a seemingly counterintuitive result: BIDZ can increase as UCS rises because, in the sensitivity setup, UCS was increased while tensile strength was kept constant.

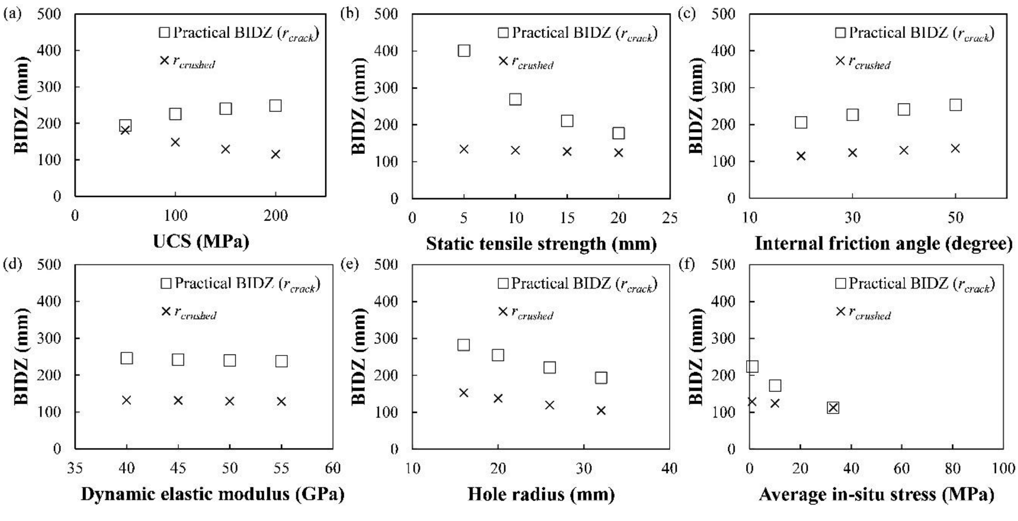

Fig. 4. Sensitivity analysis of BIDZ and r_{crack} in concentrated charge with respect to (a) UCS, (b) Static tensile strength, (c) Internal friction angle, (d) Dynamic elastic modulus, (e) Hole radius, (f) Average in-situ stress

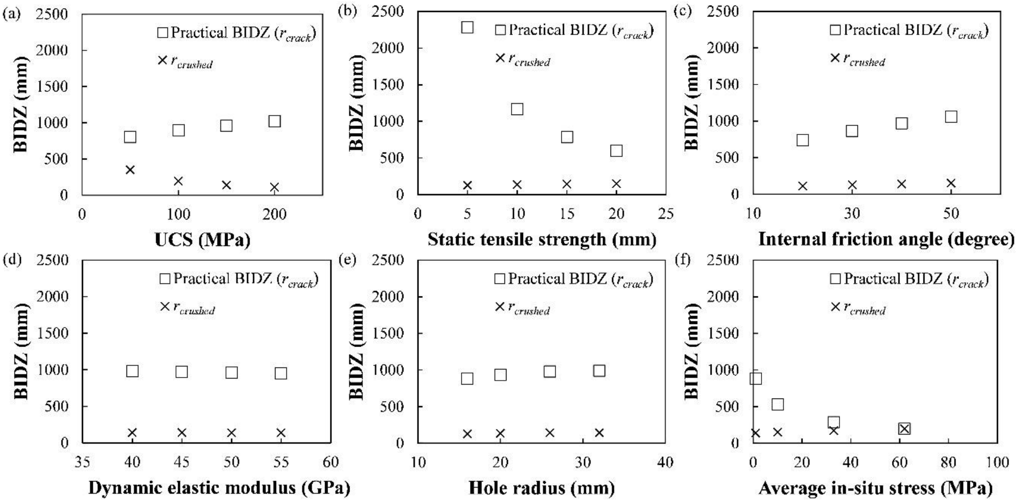

Fig. 5. Sensitivity analysis of BIDZ and r_{crack} in column charge with respect to (a) UCS, (b) Static tensile strength, (c) Internal friction angle, (d) Dynamic elastic modulus, (e) Hole radius, (f) Average in-situ stress

TABLE 4

Properties of granitic gneiss and emulsion of field-scale experiment

Site ID	Uniaxial compressive strength (MPa)	Tensile strength (MPa)	P-wave velocity (m/s)	S-wave velocity (m/s)	Rock Density (kg/m^3)	Friction angle (°)	r_{crack} (mm)	Max crack length (mm)
PF-1	106.3	12.6	5603.6	3102.8	2855	51*	243	316
PF-2	148.2	12.2	3988.2	2489.7	2658	51*	232	302

Unexploded explosive density (kg/m^3)	Ideal detonation velocity (m/s)	Complete reaction heat (kJ/kg)	Hole radius (mm)	Charge radius (mm)
1200	5900	4602	22.5	16

* assumed.

3. Methodology for field-scale pre-fracturing experiment

3.1. Site description and investigation

A field-scale pre-fracturing experiment was conducted at a quarry in Gapyeong, Korea. Two rock faces located within ~200 m were selected: PF-1, composed of biotitic gneiss, and PF-2, composed of granitic gneiss. The rock mass is moderately weathered but only sparsely fractured, with RMR > 60.

Rock cores were extracted from within the design contour before and after blasting, and laboratory tests were performed to assess blast-induced changes in rock properties. The rock faces were scanned pre- and post-blast using the LiDAR sensor on an iPhone 12 Pro to document the as-drilled pattern and surface damage [48].

3.2. Blast design of pre-fracturing in field-scale experiment

The primary explosive used was emulsion (0.16 kg × 200 mm × Φ32 mm). Non-electric detonators were utilized as in-hole detonators, arranged to initiate in a concentric sequence from the central blast area to the contour. Vibrations were measured using six devices of SV-1 of SV Corporation horizontally aligned at approximately 10-meter intervals in a straight line from the blast source [49].

The basic design of the blast pattern was based on the empirical formula proposed by Hauser. Adjustments were made to certain constants considering domestic blasting conditions and experts' experience. Burn-Cut was applied with multiple uncharged small holes at the center to increase the free face. The blast design is illustrated in Fig. 6. The charge per hole was 0.24 kg (=1.5 EA explosives), and the specific charge amounts for PF-1 and PF-2 were 0.448 and 0.397 kg/m^3, respectively.

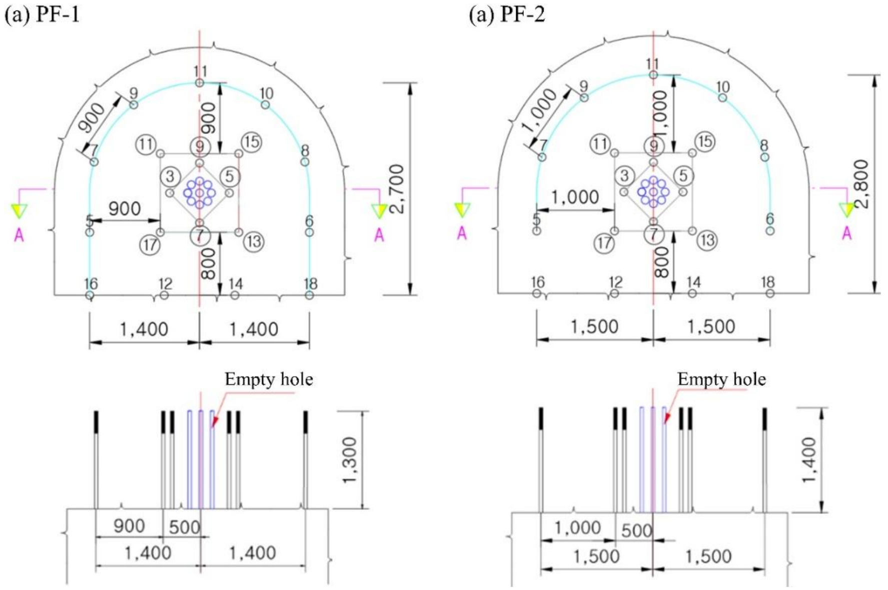

Fig. 6. Designs of pre-fracturing method in field-scale experiment in Gapyeong. (a) PF-1, (b) PF-2

4. Results and discussion

4.1. Results of the field-scale experiment

4.1.1. Rock weakening on surface observation

The pre-fracturing weakened the part of the rock face by inducing fractures, as shown in Fig. 7. Wedge-shaped fracturing due to pre-existing joints occurred on the left blast face of PF-1 (Figs. 7(b) and 7(d)), while new cracks were observed to develop around the joint crossing the upper right blast face of PF-2 (Fig. 7(h)). Additionally, Fig. 7(c) indicates that radial cracks formed around the blast hole, unaffected by the existing joints. Furthermore, in both PF-1 and PF-2, distinct fracturing was observed at the centre where holes were closely spaced. In contrast, other areas with wider hole spacings only exhibited the extension of pre-existing joints without inducing new fractures. This illustrates the visible outcomes of pre-fracturing relative to the spacing of the blast holes.

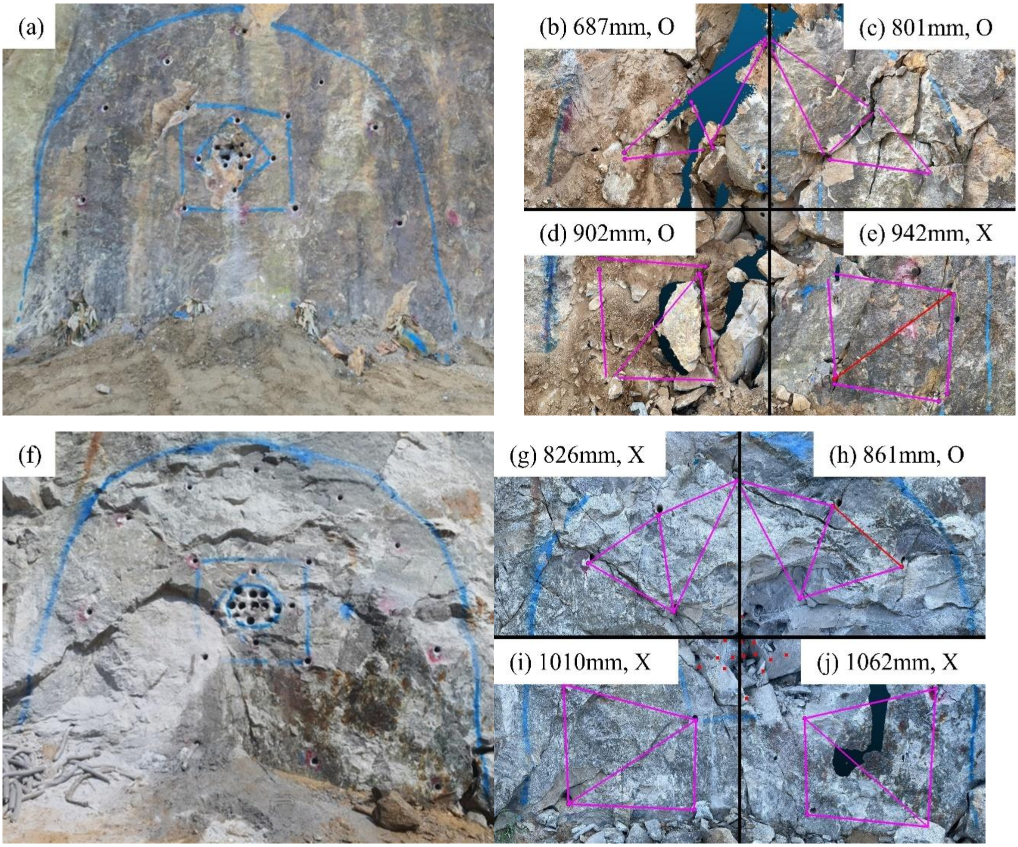

Fig. 7. Application of pre-fracturing method in PF-1 (a) before and (b)-(e) after blasting and in PF-2 (f) before and (g)-(j) after blasting. Numbers denote the average hole spacing, and O/X indicate the success/failure of weakening the rock

4.1.2. Rock weakening in laboratory test

Changes in rock properties also indicate the effect of pre-fracturing. The rock face was cored before and after pre-fracturing, and several laboratory tests were performed. Fig. 8(a) shows a decreasing trend of rock properties after blasting. However, the decrease of rock properties is not pronounced in Fig. 8(b), probably due to the large hole spacing in PF-2. The results of this test are consistent with surface observations.

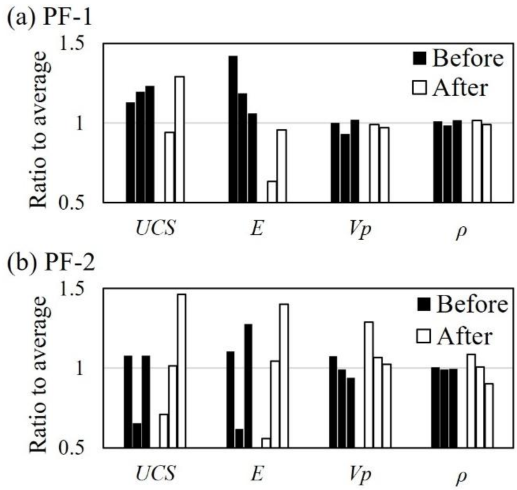

Fig. 8. Ratios of rock properties to the average values in TABLE 4 before and after pre-fracturing. (a) PF-1, (b) PF-2

4.1.3. EDZ control by vibration measurement

The EDZ was effectively controlled within approximately 10 cm from the contour using pre-fracturing. Pre-fracturing generates the BIDZ starting at the outermost blast hole and extending into the rock mass, whereas mechanical excavation follows the design contour and therefore forms its damaged zone inward from that contour. Accordingly, if the BIDZ is shorter than the sum of the distance from the outermost hole to the contour and the EDZ produced by mechanical excavation, the final EDZ is governed by mechanical excavation; if the BIDZ is longer, the final EDZ is governed by pre-fracturing. In this study, the EDZ is taken to be the damage produced by pre-fracturing alone (mechanical excavation was not performed), because the EDZ generated by mechanical excavation is comparatively small and can be neglected for the present purpose [50]. The estimation of EDZ was conducted using Eq. (24) [51], derived from the PPV-distance relationship of Eq. (22) [11] and the critical peak particle velocity defined in Eq. (23) by linking peak particle velocity to peak tensile strain and adopting a conservative tensile-failure criterion [52].

$$PPV = A\left(\frac{R}{\sqrt[3]{Q}}\right)^{a} \tag{22}$$

$$PPV_c = \sigma_t \frac{V_P}{E} \tag{23}$$

$$R_c = \left(\frac{PPV_c}{A}\right)^{\frac{1}{a}} \sqrt[3]{Q} \tag{24}$$

Where R is the distance between the blast hole and the measurement point (m), σ_t represents tensile strength (MPa), V_P is the P-wave velocity (m/s), E is Young's modulus (GPa), and Q represents the maximum charge per delay (kg/delay). In this study, due to limited tests, the constant a in Eq. (22) was fixed at –1.6 as a commonly used assumption, and only A was optimised, as shown in Fig. 9. The results show R_c of 40 cm and 39 cm from blast holes for PF-1 and PF-2, corresponding to the EDZ size of 10 cm and 9 cm from the contour. It is similar to the estimates of maximum crack length for PF-1 and PF-2 with less than 25% discrepancy (TABLE 4). Both PPV-based and BIDZ-based equations of EDZ size are not dependent on hole spacing, and the effect of hole spacing was not pronounced in this study, probably due to the large spacing. The pre-fracturing, by offsetting blast holes from the contour and utilising light charging, effectively constrained the EDZ compared to both mechanical excavation and drill and blast, which typically produces an EDZ of 0-0.3 m and 0-2 m, respectively [50]. Therefore, the combined application of mechanical excavation and pre-fracturing shows potential for effectively controlling the extent of the EDZ.

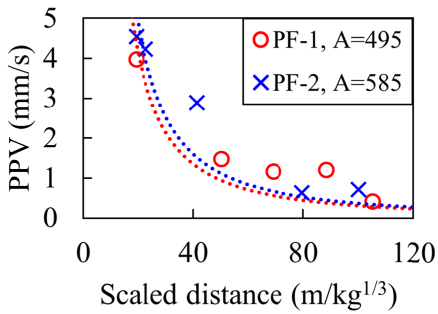

Fig. 9. Peak particle velocity versus scaled distance using the cube root of charge per delay.
(red) PF-1 and (blue) PF-2

4.2. Optimal hole spacing of pre-fracturing

The hole spacing of pre-fracturing is proposed based on the practical BIDZ model by analysing cases of conventional pre-splitting [45,53,54] and current field-scale demonstration. Cylindrical symmetry was assumed for pre-splitting cases, while spherical symmetry was assumed for the current experiment because of the concentrated charge. According to Fig. 10, when the spacing exceeds 3 times the BIDZ estimate, under-excavation or insufficient weakening of the rock mass occurred. In conventional pre-splitting, the spacing is set to be less than 1.5 times the BIDZ estimate to create fracture planes connecting the boreholes. Therefore, for pre-fracturing aimed at weakening the entire rock face, it is advisable to set the hole spacing between 1.5 to 3.0 times the BIDZ estimate. This result enables design modifications according to ground conditions and explosive properties, in contrast to traditional pre-splitting empirical approaches that relied solely on blast pattern geometry.

In the case of Äspö, simultaneous blasting was carried out with an error margin within 1 ms, leading to overlapping effects from adjacent blast holes, which successfully created pre-splitting even with very large spacings. Simultaneous blasting has the advantage of forming fractures over a wider spacing with the same amount of explosives in terms of fracture plane generation. However, since vibrations may be amplified due to the overlapping effects, caution is needed when applying simultaneous blasting in pre-fracturing.

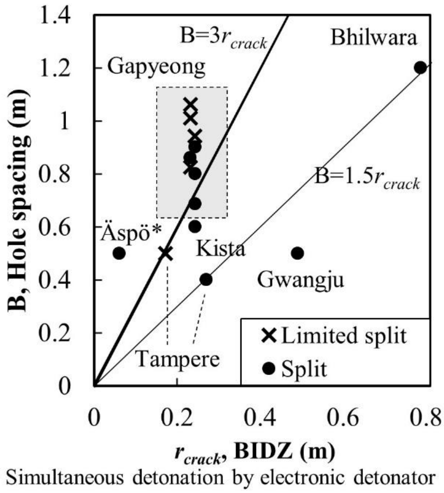

Fig. 10. Plots between hole spacing and practical BIDZ model

4.3. Proposed blast pattern of pre-fracturing and practical implication

The blast pattern of pre-fracturing is proposed based on the practical BIDZ model. The hole spacing is calculated as 1.5-3.0 times the BIDZ, and the offset from the contour is 1.3 times the BIDZ, corresponding to the maximum crack length. It allows saving explosives and reducing the extent of EDZ. The hole spacing of the contour hole is smaller than that of the inner face to ensure that the blasting effect reaches the contour evenly. As an example in Fig. 11, the entire face can be divided into equilateral triangles with sides equal to the optimal hole spacing, placing blast holes at each vertex. In actual application, a burn-cut can be applied to induce additional free faces, as applied in Fig. 6, and the charge per hole at the centre can increase to enhance

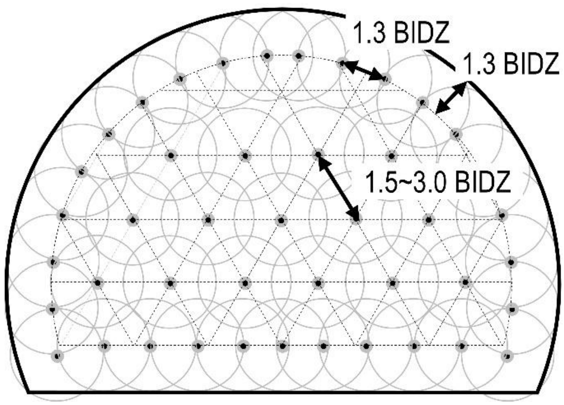

Fig. 11. Example of blasting pattern of pre-fracturing

blast efficiency. However, these additional methods inherently lead to increased vibrations, so if lower vibration thresholds are required, the use of a large-diameter cut-hole in the pattern can be considered. In addition, as the method requires a hybrid construction process integrating blast and mechanical excavation, it may pose certain disadvantages regarding the construction schedule and cost. Thus, it is recommended for use in underground spaces with specialised objectives, such as EDZ mitigation.

Field observations showed that pre-existing joints were either preferentially reactivated by blasting or acted as barriers to newly formed cracks, consistent with prior reports on joint-controlled crack evolution [55,56]. To prevent joint-controlled truncation of the BIDZ, blast holes should be offset from mapped persistent joints by a standoff on the order of one predicted BIDZ radius so that the BIDZ can develop without being clipped by the joint. Although the influence of rock anisotropy was not pronounced at this site, anisotropy is known to elongate the BIDZ along weak fabrics [57,58]. In such cases, to achieve uniform rock-face weakening, hole spacing should be governed by the minimum BIDZ radius across azimuths and the blast pattern adjusted accordingly.

5. Conclusion

Pre-fracturing is an auxiliary method for mechanical excavation to weaken hard rock and control the EDZ. The first objective was to develop and validate a practical, quasi-static model that estimates the BIDZ around a single borehole, accounting for dynamic rock strength, in-situ stress, spherical symmetry of a concentrated charge, and blasting-induced changes in hole radius; the plausibility of the quasi-static assumption was also examined. The second objective was to translate this model into a pre-fracturing design methodology aimed at rock-face weakening and EDZ control. Accordingly, the study addressed two questions: (i) how the BIDZ estimate relates to the effective damage extent (EDZ/maximum crack length), and (ii) what BIDZ-normalised hole-spacing threshold governs whether weakening is achieved. Comparisons between the practical BIDZ model and dynamic numerical models showed similar trends, with discrepancies of less than 45%, supporting the practical applicability of the quasi-static assumption. Empirical relations of hole-spacing design in Canada and BIDZ estimation in Sweden aligned well with the proposed practical model. Based on experimental data from Finland and Sweden, the maximum crack length from a blast hole was, on average, approximately 1.3 times the BIDZ estimated by the practical model, probably due to strength heterogeneity. The correlation of the practical model was comparable to that of the empirical models, providing further validation. Field-scale demonstrations of pre-fracturing were conducted at a rock slope in a quarry. Rock weakening with decreasing hole spacing was validated through surface observations and laboratory tests, while the EDZ extent, assessed via PPV measurements, was effectively controlled to remain below the extent typically associated with conventional excavation methods. In addition, the EDZ extent was comparable to the maximum crack length inferred from the BIDZ estimate. By combining data on hole spacing from existing pre-splitting cases and the field-scale demonstration, an optimal hole spacing for pre-fracturing was proposed to be 1.5-3.0 times the BIDZ estimated by the practical model. Furthermore, a blast-pattern design for pre-fracturing is suggested based on the optimal hole spacing and the maximum crack length estimated by the practical BIDZ model. In practice, a burn cut, a higher central charge, or a large diameter cut hole can improve efficiency. Because the pre-fracturing integrates blasting with mechanical excavation and can affect schedule and cost, pre-fracturing is best applied in underground works with specialised goals such as EDZ mitigation.

Acknowledgements

This work was supported by the Institute for Korea Spent Nuclear Fuel (iKSNF) and Korea Institute of Energy Technology Evaluation and Planning (KETEP) grant funded by Ministry of Trade, Industry and Energy (MOTIE) of the Korean government (No. RS-2023-KP002657).

Reference

[1] C.P. Nathanail, Assessments of ease of blasting in Troodos Sheeted Dyke Complex and Lower Pillow Lava Series. Geol. Soc. Emg. Geol. S.P. **10** (1), 355-359 (1995). DOI: https://doi.org/10.1144/gsl.eng.1995.010.01.31

[2] J.A. Franklin, E. Broch, G. Walton, Logging the mechanical character of rock. T. I. Min. Metall. A. **80**, (1971).

[3] Q. Yan, M. Sun, C. Yao, H. Liu, W. Wu, J. Duan, A method for detecting and pretreating boulders during shield tunneling in granite strata. B. Eng. Geol. Environ. **80**, 3009-3022 (2021). DOI: https://doi.org/10.1007/s10064-021-02103-x

[4] X. Wang, J. Xu, W. Zhu, Y. Li, Roof pre-blasting to prevent support crushing and water inrush accidents. Int. J. Min. Sci. Technol. **22** (3), 379-384 (2012). DOI: https://doi.org/10.1016/j.ijmst.2012.04.016

[5] A.Z. Toper, K.K. Kabongot, R.D. Stewart, A. Daehnke, The mechanism, optimization and effects of preconditioning. J. S. Afr. I. Min. Metall. **100** (1), 7-15 (2000). DOI: https://hdl.handle.net/10520/aja0038223x_2586

[6] C. Drover, E. Villaescusa, I. Onederra, Face destressing blast design for hard rock tunnelling at great depth. Tunn. Undergr. Sp. Tech. **80**, 257-268 (2018). DOI: https://doi.org/10.1016/j.tust.2018.06.021

[7] F. Sengani, Fundamental principles of rock fracturing at the vicinity of preconditioned blast hole. Arch. Min. Sci. **65** (4), 769-786 (2020). DOI: https://doi.org/10.24425/ams.2020.134146

[8] A. Saadatmand Hashemi, P. Katsabanis, Tunnel face preconditioning using destress blasting in deep underground excavations. Tunn. Undergr. Sp. Tech. **117**, 104126 (2021). DOI: https://doi.org/10.1016/j.tust.2021.104126

[9] Dynonobel, Blasting and Explosives Quick Reference Guide, Dyno Nobel Asia Pacific Pty Limited, Kalgoorlie (2010).

[10] W. Hustrulid, Blasting principles for open pit mining: Volume 2 – Theoretical foundations. AA Balkema, Rotterdam (1999).

[11] R. Holmberg, P.A. Persson, Design of tunnel perimeter blasthole patterns to prevent rock damage. T. I. Min. Metall. A. **89**, (1980). DOI: https://doi.org/10.1016/0148-9062(80)90767-6

[12] M.F. Drukovanyi, V.S. Kravtsov, Y.E. Chernyavskii, V.V. Shelenok, N.P. Reva, S.N. Zerk'kov, Calculation of fracture zones created by exploding cylindrical charges in ledge rocks. Sov. Min. Sci. **12**, 292-295 (1976). DOI: https://doi.org/10.1007/BF02594873

[13] A.A. Il'yushin, Mechanics of a continuous medium, Izd-vo MGU, Moscow (1971).

[14] V.M. Senuk, The impulse from an explosion, and conditions for its greater utilization in crushing hard rock masses in blasting. Sov. Min. Sci. **15**, 22-27 (1979). DOI: https://doi.org/10.1007/bf02499637

[15] SNRA, Cautious blasting careful blasting and scaling, rock engineering directions for the construction of Ringen and Yttre Tvärleden, Stockholm (1995).

[16] F. Ouchterlony, Prediction of crack lengths in rock after cautious blasting with zero inter-hole delay. Fragblast **1** (4), 417-444 (1997). DOI: https://doi.org/10.1080/13855149709408407

[17] P.A. Persson, R. Holmberg, J. Lee, Rock blasting and explosives engineering, CRC press (1994). DOI: https://doi.org/10.5860/choice.31-5469

[18] Atlas Powder, Explosives and rock blasting, Dallas (1987).

[19] S. Esen, I. Onederra, H.A. Bilgin, Modelling the size of the crushed zone around a blasthole. Int. J. Rock. Mech. Min. **40** (4), 485-495 (2003). DOI: https://doi.org/10.1016/s1365-1609(03)00018-2

[20] S. Nie, Measurement of borehole pressure history in blast holes in rock blocks. Fragblast **91**(7), (1999).

[21] J.L. Workman, P.N. Calder, Wall control blasting at the Manassas Quarry. In: The Annual Conference on Explosives and Blasting Technique. International Society of Explosives Engineers, **243** (1992).

[22] W. Fickett, W.C. Davis, Detonation: Theory and Experiment. Courier Corporation (2001).

[23] W. Lu, Z. Leng, M. Chen, P. Yan, Y. Hu, A modified model to calculate the size of the crushed zone around a blasthole. J. S. Afr. I. Min. Metall. **116** (5), 412-422 (2016). DOI: https://doi.org/10.17159/2411-9717/2016/v116n5a7

[24] Q. Xu, Z.Q. Wang, The Comparative Study on the Damage Zones of Cylindrical and Spherical Charges in Rock and Soil. Shock. Vib. **2021** (1), 9971761 (2021). DOI: https://doi.org/10.1155/2021/9971761

[25] L. Dong, Y. Zhang, J. Ma, Micro-crack mechanism in the fracture evolution of saturated granite and enlightenment to the precursors of instability. Sensors **20** (16), 4595 (2020). DOI: https://doi.org/10.3390/s20164595

[26] A.K. Raina, R. Trivedi, Exploring Rock–Explosive Interaction Through Cross Blasthole Pressure Measurements. Geotechnical and Geological Engineering **37** (2), 651-658 (2019). DOI: https://doi.org/10.1007/s10706-018-0635-3

[27] A.S.P. Rae, T. Kenkmann, V. Padmanabha, M.H. Poelchau, F. Schäfer, Dynamic Compressive Strength and Fragmentation in Felsic Crystalline Rocks. J. Geophys. Res.-Planet. **125** (10), e2020JE006561 (2020). DOI: https://doi.org/10.1029/2020JE006561

[28] A.S.P. Rae, T. Kenkmann, V. Padmanabha, M.H. Poelchau, F. Schäfer, M.A. Dörfler, L. Müller, Dynamic compressive strength and fragmentation in sedimentary and metamorphic rocks. Tectonophysics **824**, 229221 (2022). DOI: https://doi.org/10.1016/j.tecto.2022.229221

[29] H. Jeong, B. Jeon, S. Choi, S. Jeon, Fracturing behavior around a blasthole in a brittle material under blasting loading. Int. J. Impact Eng. **140**, 103562 (2020). DOI: https://doi.org/10.1016/j.ijimpeng.2020.103562

[30] G. Liu, X. Li, Z. Peng, W. Chen, Experimental Investigation on the Influence of Water on Rockburst in Rock-like Material with Voids and Multiple Fractures. Materials **17** (12), 2818 (2024). DOI: https://doi.org/10.3390/ma17122818

[31] R. Xu, Y. Hu, Z. Yan, Y. Zhao, Z. Li, Experimental Investigation on the Effect of Water Saturation on the Failure Mechanism and Acoustic Emission Characteristics of Sandstone. Int. J. Geomech. **24** (6), 04024102 (2024). DOI: https://doi.org/10.1061/ijgnai.gmeng-8526

[32] Y. Zhou, W. Lv, B. Li, Q. Liang, Impact of Soft Minerals on Crack Propagation in Crystalline Rocks under Uniaxial Compression: A Grain-Based Numerical Investigation. Int. J. Numer. Anal. Methods Geomech. **48** (8), 2020-2042 (2024). DOI: https://doi.org/10.1002/nag.3718

[33] Y. Su, P. Zeng, W. Yao, J. Gao, C. Zhou, J. Duan, … Y. Li, Investigating the Dynamic Characteristics of Crack Formation of Jiangxi Lateritic Soil Subjected to Drying–Wetting Cycles. J. Saf. Sustain. (2025). DOI: https://doi.org/10.1016/j.jsasus.2025.06.005

[34] P. Calder, Pit Slope Manual Chapter 7 – Perimeter Blasting, Ottawa (1977).

[35] C. Sjöberg, B. Larsson, M. Lindstrom, K. Palmqvist, A blasting method for controlled crack extension and safety underground. ASF Project No. 77/224. Nitro Consult. Gothenburg (1977).

[36] C. Sjöberg, Cracking zones around slender borehole charges. In: Annual Discussion Meeting BK-79, Swedish rock construction committee, Stockholm 53-98 (1979).

[37] F. García Bastante, L. Alejano, J. González-Cao, Predicting the extent of blast-induced damage in rock masses. Int. J. Rock Mech. Min. **56**, 44-53 (2012). DOI: https://doi.org/10.1016/j.ijrmms.2012.07.023

[38] F. Ouchterlony, M. Olsson, I. Bergqvist, Towards new Swedish recommendations for cautious perimeter blasting. Fragblast **6** (2), 235-261 (2002). DOI: https://doi.org/10.1076/frag.6.2.235.8666

[39] M. Olsson, J. Svärd, F. Ouchterlony, Sprängskador från strängemulsion: fältförsök och förslag till skadezonstabell som innehåller samtidig upptändning. Stockholm (2008).

[40] M. Olsson, I. Bergqvist, Crack growth in rock during cautions blasting. SveBeFo report no. 3, Swedish Rock Engineering Research. Stockholm (1993).

[41] M. Olsson, I. Bergqvist, Crack growth during multiple hole blasting. SveBeFo report no.18, Swedish Rock Engineering Research, Stockholm (1996).

[42] X. Yang, D. Yuan, H. Xue, Y. Gao, X. Tian, J. Qi, L. Hou, J. Cao, Research on Roof Cutting and Pressure Releasing Technology of Cumulative Blasting in Deep and High Stress Roadway. Geotech. Geol. Eng. **39** (3), 2653-2667 (2021). DOI: https://doi.org/10.1007/s10706-020-01649-z

[43] M. Olsson, F. Ouchterlony, New formula for blast induced damage in the remaining rock. SveBeFo report no. 65, Swedish Rock Engineering Research, Stockholm (2003).

[44] H. Ittner, B. Wenby, A. Bouvin, T. Husaas, Investigation of blast fractures from mechanized charging with emulsion during tunnelling. In: ITA-AITES World Tunnel Congress, International Tunneling and Underground Space Association, Bergen (2017): pp. 1542-1549.

[45] H. Ittner, Excavation damage from blasting with emulsion explosives: Quality control and macro fracturing in the remaining rock. Doctoral dissertation, Luleå University of Technology (2018).

[46] J.U.S. Jokinen, K. Ylätalo, The effect of loosening techniques on the product quality in the dimensional stone quarrying industry. Res. reports TK-KAL-A17 6: A-18. Laboratory of Rock Engineering. Helsinki University of Technology, Helsinki (1995).

[47] B. Afrasiabian, M. Eftekhari, Prediction of mode I fracture toughness of rock using linear multiple regression and gene expression programming. Journal of Rock Mechanics and Geotechnical Engineering **14** (5), 1421-1432 (2022). DOI: https://doi.org/10.1016/j.jrmge.2022.03.008

[48] J. Yim, J.H. Jung, H.B. Kang, J.W. Lee, Y.J. Shin, Application of Pre-Fracturing Blast for Blast-Induced Damaged Zone Control. Tunnel Undergr. Space **34(**5), 421–432 (2024). DOI: https://doi.org/10.7474/TUS.2024.34.5.421

[49] J. Yim, B.C. Lee, J.H. Jung, H.B. Kang, J.W. Lee, Y.J. Shin, Field Demonstration of Pre-Fracturing for Controlling Noise and Vibration. Explosives and Blasting **42** (3), 49-57 (2024).
DOI: https://doi.org/10.22704/ksee.2024.42.3.049

[50] J. Yoon, K.-B. Min, S. Kwon, M.K. Song, S.S. Lee, T.Y. Ko, H. Jeong, Y. Shin, J. Jung, J. Yim, Oversea & Domestic Case Studies on Excavation Damaged Zone for Deep Geological Repository for Spent Nuclear Fuel. Tunnel Undergr. Space **34** (1), 15-27 (2024). DOI: https://doi.org/10.7474/tus.2024.34.1.015

[51] S. Kwon, C.S. Lee, S.J. Cho, S.W. Jeon, W.J. Cho, An Investigation of the Excavation Damaged Zone at the KAERI Underground Research Tunnel. Tunn. Undergr. Space Technol. **24** (1), 1-13 (2009).
DOI: https://doi.org/10.1016/j.tust.2008.01.004

[52] W.W. Forsyth, A Discussion of Blast-Induced Overbreak Around Underground Excavation. In: Proc. 4th Int. Symp. on Rock Fragmentation by Blasting (FRAGBLAST-4), Vienna (1993): pp. 161-166.

[53] I.-J. Kim, Y.-S. Kim, K.-C. Ki, A Tunnel Blasting Method Favorable to the Environment, Which Utilizes Pre-Splitting & an Upper Center Cut. Explosives and Blasting **20** (2), 7-19 (2002).

[54] P.K. Singh, M.P. Roy, R.K. Paswan, Controlled blasting for long term stability of pit-walls. Int. J. Rock Mech. Min. **70**, 388-399 (2014). DOI: https://doi.org/10.1016/j.ijrmms.2014.05.006

[55] J. Ge, Y. Jia, W. Huang, M. Yu, S. Ni, Y. Xu, K. Gu, Analysis on Characteristics and Mechanism for Rock Fracture in Deep Rock with Cracks under Dynamic-Static Coupling Effect. Sci. Rep. **14**, 31840 (2024).
DOI: https://doi.org/10.1038/s41598-024-83256-z

[56] C. Xiao, R. Yang, J. Zuo, J. Chen, J. Zhao, Y. Yang, Influence of Open Joints on Blasting Damage and Crack Propagation of PMMA. Mech. Adv. Mater. Struct. **31** (15), 3204-3215 (2024).
DOI: https://doi.org/10.1080/15376494.2023.2171166

[57] C. Chu, S. Wu, C. Zhang, Y. Zhang, Microscopic Damage Evolution of Anisotropic Rocks under Indirect Tensile Conditions: Insights from Acoustic Emission and Digital Image Correlation Techniques. Int. J. Miner. Metall. Mater. **30** (9), 1680-1691 (2023). DOI: https://doi.org/10.1007/s12613-023-2649-y

[58] Q. Dong, H. Tong, J. Sun, S. Peng, J. Jia, Experimental Study of the Dynamic Compressive and Tensile Anisotropic Mechanical Properties and Failure Modes of Shale. Sensors **25** (9), 2905 (2025).
DOI: https://doi.org/10.3390/s25092905